npj | vaccines

Article

Published in partnership with the Sealy Institute for Vaccine Sciences

https://doi.org/10.1038/s41541-024-00954-5

An attachment glycoprotein nanoparticle elicits broadly neutralizing antibodies and protects against lethal Nipah virus infection

Dan Zhou[1,5], Rao Cheng[1,5], Yanfeng Yao[2,5], Gan Zhang[1], Xin Li[1], Bingjie Wang[1], Yong Wang[3,4], Feiyang Yu[1], Shangyu Yang[1], Hang Liu[2], Ge Gao[2], Yun Peng[2], Miaoyu Chen[2], Zengqin Deng[3,4] ✉ & Haiyan Zhao[1] ✉

Nipah virus (NiV) is a zoonotic emergent paramyxovirus that can cause severe encephalitis and respiratory infections in humans, with a high fatality rate ranging from 40% to 75%. Currently, there are no approved human vaccines or antiviral drugs against NiV. Here, we designed a ferritin-based self-assembling nanoparticle displaying the NiV G head domain on the surface (NiV G-ferritin) and assessed immune responses elicited by the soluble NiV G head domain (NiV sG) or NiV G-ferritin. Immunization with NiV G-ferritin or NiV sG conferred complete protection against lethal NiV challenge without detection of viral RNA in Syrian golden hamsters. Compared to NiV sG, NiV G-ferritin induced significantly faster, broader, and higher serum neutralizing responses against three pathogenic henipaviruses (NiV-Malaysia, NiV-Bangladesh, and Hendra virus). Moreover, NiV G-ferritin induced a durable neutralizing immunity in mice as antisera potently inhibited NiV infection even after six months of the third immunization. Additionally, we isolated a panel of 27 NiV G-binding monoclonal antibodies (mAbs) from NiV G-ferritin immunized mice and found that these mAbs targeted four distinct antigenic sites on NiV G head domain with two sites that have not been defined previously. Notably, 25 isolated mAbs have potent neutralizing activity with 50% inhibitory concentrations less than 10 ng/mL against NiV pseudovirus. Collectively, these findings provide new insights into the immunogenicity of NiV G protein and reveal that NiV G-ferritin is a safe and highly effective vaccine candidate against Nipah virus infection.

Nipah virus (NiV) is a negative-sense, single-stranded RNA virus that was initially isolated and identified during an outbreak in Malaysia and Singapore from 1998 to 1999[1,2]. Since the first outbreak, there were few cases of NiV in either Malaysia or Singapore until 2001, from when NiV outbreaks were nearly annual events in Bangladesh[3,4]. Most recently, the outbreak of NiV occurred in Kerala, India, in 2023, with six infected individuals resulting in 2 deaths[5]. NiV infection can cause severe encephalitis and respiratory disease, with a case fatality rate up to 75%. In addition, long-term neurological conditions and relapse of NiV infection have also been observed in survivors[6,7]. Currently, no approved vaccines or therapeutics are available for humans.

NiV belongs to the genus of *Henipavirus* (HNV) in the family *Paramyxoviridae*, which also includes another highly pathogenic virus, Hendra virus (HeV)[8]. In addition, new henipavirus-like viruses have been continuously reported recently, like Cedar virus (CedV)[9], Ghana virus (GhV), Mòjiāng virus (MojV)[10], and Langya virus (LayV)[11]. Two NiV lineages are identified based on viral geographic distributions and genetic diversity: NiV Malaysia (NiV-M) and NiV Bangladesh (NiV-B)[12]. NiV has a broad host

[1]State Key Laboratory of Virology, College of Life Sciences, Wuhan University, Wuhan, Hubei, China. [2]Center for Biosafety Mega-Science, Wuhan Institute of Virology, Chinese Academy of Sciences, Wuhan, Hubei, China. [3]Key Laboratory of Virology and Biosafety, Wuhan Institute of Virology, Chinese Academy of Sciences, Wuhan, Hubei, China. [4]Hubei Jiangxia Laboratory, Wuhan, Hubei, China. [5]These authors contributed equally: Dan Zhou, Rao Cheng, Yanfeng Yao. ✉e-mail: dengzengqin@wh.iov.cn; hy.zhao@whu.edu.cn

tropism, including bats, pigs, dogs, cats, horses, guinea pigs, and hamsters[13]. Humans are predominantly infected through contact with infected animals (such as bats and pigs) and consuming contaminated food, although direct human-to-human transmission has also been regularly reported[6,7], highlighting the concern about potential HNV risk to global health. World Health Organization (WHO) has listed HNV infections as priority diseases requiring extensive and exigent research into the development of countermeasures[14].

NiV encodes two viral membrane proteins, glycoprotein (G) and fusion protein (F), which are situated on the viral surface and function in a concerted manner to help the virus enter the target cells and initiate infection. Previous studies showed that tyrosine kinases ephrin-B2 and ephrin-B3 are receptors of NiV and HeV, and the G protein is accountable for receptor recognition and binding[15,16]. After receptor engagement, the G protein undergoes a cascade of conformational changes, which could activate the F protein to start and complete membrane fusion with target cells[17,18]. In addition, many neutralizing and protective antibodies primarily target G and F proteins, indicating that the two viral proteins are key antigens for vaccine development.

Multiple vaccine platforms against NiV infection have been developed recently, which include subunit vaccines[19,20], mRNAs[21], virus-like particles (VLPs)[22], viral vector vaccines[23–29], and DNA vaccines[26], whereas no self-assembling nanoparticle platform has been assessed for NiV infection. As a nanoparticle vaccine carrier, ferritin can self-assemble into an octahedral cage with 24 identical subunits arranged around and display the antigen multivalently[30]. The antigen multimerization property of nanoparticles likely allows multivalent binding of B cell receptors and thus benefits the B-cell activation and elicitation of robust immune responses against the delivered antigen[31–34]. Due to these advantages, this delivery system has been extensively utilized in vaccine developments against diverse infectious pathogens and tumors, including influenza vaccines[35,36], Epstein-Barr virus vaccines[37,38], and COVID-19 vaccines[39–42].

In this study, we designed and characterized a ferritin-based nanoparticle vaccine that displays the head domain of the NiV G protein (NiV G-ferritin). Immunization with the NiV G-ferritin induced a rapid, robust, and long-lasting humoral immune response against NiV in mice, which is significantly better than immunization with the soluble NiV G head domain (NiV sG). Furthermore, three-dose vaccination with NiV G-ferritin or NiV sG could completely protect Syrian golden hamsters from lethal NiV infection. We also isolated 27 anti-NiV-G monoclonal antibodies (mAbs) with diverse inhibitory activities against NiV infection and found that these mAbs recognize four distinct antigenic sites on NiV G, including two new sites that have not been identified before. Our work provides a potential NiV vaccine candidate and demonstrates that the G head domain is an excellent antigen for NiV vaccine development.

Results

Design and generation of NiV G nanoparticle immunogen

Previous studies have shown that the receptor binding site is located on the NiV G head domain, which is targeted by most neutralizing and protective mAbs. Among the reported self-assembling nanoparticle systems, *Helicobacter pylori*-bullfrog hybrid ferritin (simplified as ferritin) was selected as it can minimize vaccine-induced autoimmunity and ferritin-displayed immunogens can confer stronger immunity in animals toward other viruses[38,41]. To uniformly display the NiV G head domain on the surface of ferritin, the C-terminal of the NiV G (residues:176–602) was fused to the N-terminal extension of ferritin (designated NiV G-ferritin hereafter). The signal peptide was fused to the N-terminal of NiV G head domain for eukaryotic secretion expression in Expi293F cells.

Since the antigenicity of the NiV G head domain as a soluble protein or in the context of the ferritin nanoparticle might be different, we also expressed and purified NiV sG using the same system. Meanwhile, ferritin alone without the antigen was also included as a negative control (Fig. 1a). Size-exclusion chromatography (SEC) profiles showed that NiV G-ferritin was eluted in an earlier peak than either ferritin alone or NiV sG (Fig. 1b), indicating the successful assembly of NiV G nanoparticle. SDS-PAGE analysis showed that NiV G-ferritin, NiV sG and ferritin gave highly pure bands around 70 kDa, 50 kDa and 19 kDa, respectively, which are close to their respective predicted molecular weights of monomeric form (Fig. 1c). We further determined the molecular weights of NiV G-ferritin and NiV sG by size-exclusion chromatography coupled with multiangle light scattering (SEC-MALS). The calculated molecular weight of the protein component of NiV G-ferritin is approximately 1.5 MDa, corresponding to ~21× monomeric NiV G-ferritin, suggesting that NiV G-ferritin multivalently presents the G head domain. The average protein component molecular weight of NiV sG is 48.8 kDa, consistent with the expected molecular weight (48.7 kDa) (Fig. 1d).

Characterization and antigenic feature of NiV G-ferritin

We next examined the overall structures of ferritin alone and NiV G-ferritin by negative-stain electron microscopy (nsEM). The nsEM graphs showed that both ferritin and NiV G-ferritin formed dispersed spherical particles with no evidence of aggregation (Fig. 1e). The 2D classification averages clearly show that the surface of NiV G-ferritin was spike-like compared to ferritin alone (Fig. 1e), and the measured diameters of NiV G-ferritin and ferritin assembled particles were ~22 nm and ~12 nm, respectively, suggesting that the NiV G head domain is displayed on the surface of the ferritin nanoparticle. The dynamic light scattering (DLS) analysis showed that the hydrodynamic diameter of NiV G-ferritin (~29.4 nm) was much larger than that of NiV sG (~12.7 nm) and ferritin alone (~23.5 nm) (Fig. 1f). The inferred polydispersity index (PDI) of NiV G-ferritin was less than 10%, indicating a homogeneous distribution in size (Fig. 1f). The differential scanning fluorimetry (DSF) results showed that NiV G-ferritin and NiV sG exhibit similar thermal stability with a Tm of ~65 °C, indicating that the fusion of NiV G and ferritin has no significant effect on its structural stability (Fig. 1g).

Next, we used previously reported antibodies HENV-32, HENV-26, and nAH1.3 to test the antigenicity of NiV G-ferritin. HENV-26 recognizes the receptor binding site on the head domain of the G protein, while HENV-32 and nAH1.3 have two distinct binding footprints on the G protein and do not compete with HENV-26 or viral receptor ephrin-B2[43,44]. Enzyme-linked immunosorbent assay (ELISA) results showed that antibodies HENV-32, HENV-26, or nAH1.3 could interact with NiV G-ferritin as well as NiV sG. As expected, no binding signal was observed for the negative control antibody (RVC20), which is a reported anti-Rabies virus mAb[45], indicating that the reactivity of NiV G-ferritin to these three antibodies was similar to that of NiV sG (Fig. 1h).

NiV G-ferritin elicits strong antibody responses in mice

To evaluate the immunogenicity of NiV G-ferritin, we intramuscularly immunized BALB/c mice three times with AddaVax-adjuvanted NiV G-ferritin, NiV sG, or ferritin alone and collected sera throughout the immunization process (Fig. 2a). Immunization doses were calculated according to the assembly of the nanoparticle and molecular weight of the NiV G head domain to ensure an equivalent amount of G protein was used for direct comparison. Mice were immunized with either 1 μg or 10 μg NiV sG, or NiV G-ferritin containing corresponding amounts of NiV G head domain. Blood was collected weekly (Days 7, 14, and 21) after the prime and three weeks post the second and third immunizations (Days 42 and 61) for detection of NiV G-binding IgG titers (half-maximal effective concentrations [EC_{50}]) and neutralization titers (half-maximal inhibitory concentrations [NT_{50}]).

Surprisingly, the NiV G-binding IgG (geometric mean EC_{50}, 1:157 for 1 μg group and 1:399 for 10 μg group) and pseudovirus-neutralizing titers (geometric mean NT_{50}, 1:54 for 1 μg group and 1:178 for 10 μg group) were detected seven days after the first immunization with NiV G-ferritin in mouse sera (Fig. 2b, c). In contrast, NiV G-binding IgG and pseudovirus-neutralizing titers were below the detection limit in sera of NiV sG-immunized mice seven days post the first immunization, suggesting that the NiV G nanoparticle is more immunogenic than NiV sG in vaccinated mice.

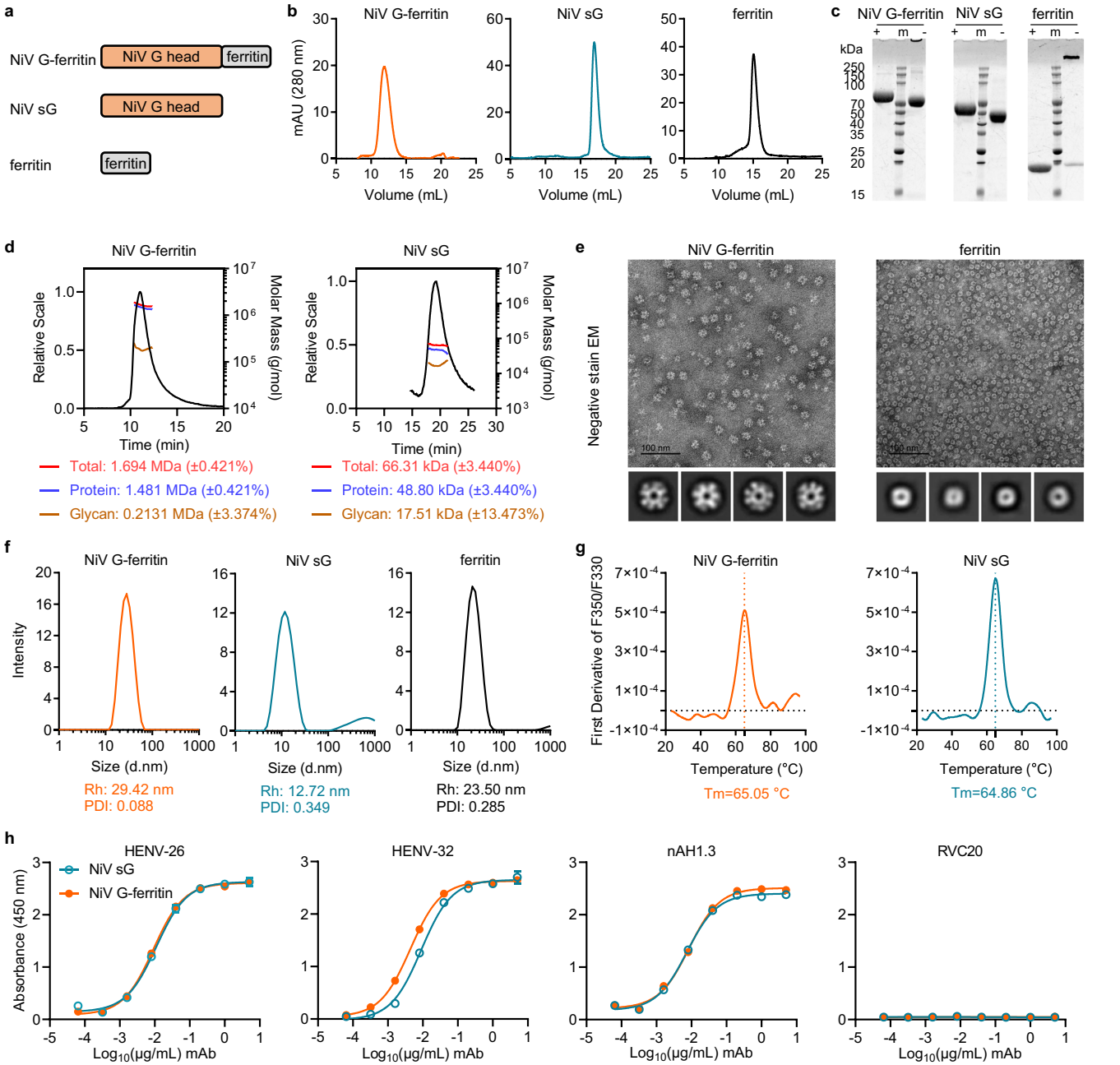

Fig. 1 | Design and characterization of NiV G nanoparticle. a Schematic of NiV G nanoparticle (NiV G-ferritin), soluble NiV G head domain (NiV sG), and ferritin proteins. **b** SEC of NiV G-ferritin, NiV sG, and ferritin on Superose 6 Increase 10/300GL. **c** SDS-PAGE analysis of NiV G-ferritin, NiV sG, and ferritin under reduced (left) and non-reduced (right) conditions. The gels were derived from the same experiment and processed in parallel. **d** Size exclusion chromatography coupled with multi-angle light scattering (SEC-MALS) analysis of NiV G-ferritin and NiV sG. The SEC-MALS shows the protein component molecular weight (blue line) of NiV G-ferritin and NiV sG is ~1.5 MDa and 48.8 kDa, respectively. **e** Negative-stain electron micrographs and 2D classification averages of purified NiV G-ferritin and ferritin nanoparticle immunogens. Scale bar, 100 nm. **f** Hydrodynamic diameter distribution of NiV G-ferritin, NiV sG, and ferritin measured by dynamic light scattering (DLS). Each protein was performed three times. The data represent the mean intensity from three replications. **g** Thermal stability assay of NiV G-ferritin and NiV sG by differential scanning fluorimetry (DSF). Protein denaturation was monitored as the sample temperature increased. Each protein was performed four times, and representative data are shown. **h** Antigenicity detection of NiV G-ferritin nanoparticle using published NiV G mAbs by ELISA. HENV-26, HENV-32, and nAH1.3 are NiV G-specific mAbs targeting three distinct epitopes on NiV G. Rabies virus monoclonal antibody RVC20 was used as a negative control. The ELISA was performed twice independently, and representative binding curves are shown. Each symbol represents mean ± SEM.

Notably, during the immunization period, NiV G-ferritin induced higher pseudovirus-neutralizing and NiV G-binding IgG titers than NiV sG, in both 1 μg/dose or 10 μg/dose immunized mice (Fig. 2b–e). As immunization doses increased, the NiV G-binding IgG and pseudovirus-neutralizing titers were steadily improved in both groups, and NiV G-ferritin was more effective in eliciting NiV G-binding and neutralizing serum antibodies than NiV sG, but the difference was not statistically significant at some time points (Fig. 2b–e). To validate the pseudovirus-neutralizing data, we tested serum-neutralizing activity against authentic NiV-M virus three weeks post the last immunization (Day 61). The results showed that the serum geometric mean NT_{50} titers of NiV G-ferritin groups were higher than that of NiV sG groups (~6-fold for the 1 μg groups and 2-fold for 10 μg groups), but did not reach, statistical significance (Fig. 2f). As expected, ferritin alone failed to induce NiV-specific antibody responses (Fig. 2b–f). We did not

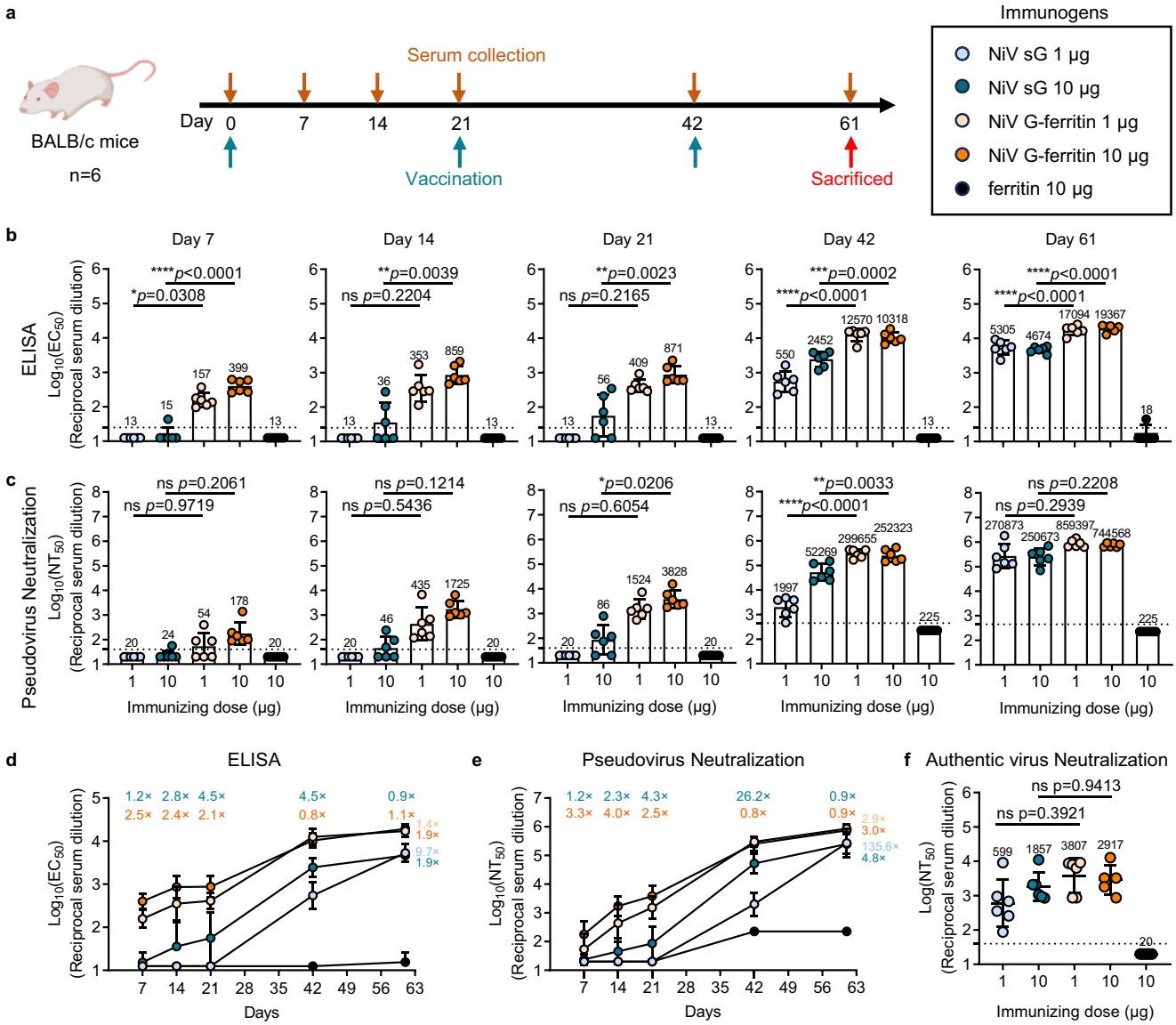

Fig. 2 | Immunogenicity of NiV sG and NiV G nanoparticle immunogens in BALB/c mice. a Schematic diagram of mice immunization. An ELISA measured the NiV G-binding IgG titers (**b**), and a NiV-M pseudovirus neutralization assay determined neutralization activity (**c**) of the sera from mice immunized with NiV sG, NiV G-ferritin, or ferritin at Days 7, 14, 21, 42 and 61 post first immunization. The numbers above the symbols indicate the geometric mean titers (GMTs). Kinetics of NiV G-binding IgG titers (**d**) and serum neutralization titers (**e**) after immunization with NiV sG, NiV G-ferritin, or ferritin. The GMTs fold change between 1 μg and 10 μg groups are shown above the curves in blue and orange for NiV sG and NiV G-ferritin immunogens, respectively. The GMTs fold change between Day 42 and Day 61 are shown on the right of the curves. **f** Serum neutralizing activity against authentic NiV Malaysia strain at Day 61 (~three weeks after the third immunization). In the 10 μg NiV G-ferritin group, a mouse serum NT_{50} exceeded the highest serum dilution (NT_{50} > 9720) and was not shown. The ELISA and pseudovirus neutralization assays were performed twice independently in duplicate wells, and representative data are shown with the half-maximal effective concentrations (EC_{50}) for ELISA and half-maximal inhibitory concentrations (NT_{50}) for neutralization determined using non-linear regression analysis. Authentic virus neutralization NT_{50} values were calculated using IBM SPSS Statistics 27. Dashed lines indicate the limit of detection (LOD) of the assays. The values lower than LOD were calculated as half of LOD. Data in each group are presented as geometric mean with geometric SD in one independent experiment. Statistical significance was determined by the one-way ANOVA with Tukey's multiple comparisons test. ns not significant, $^{*}p < 0.05$, $^{**}p < 0.01$, $^{***}p < 0.001$, $^{****}p < 0.0001$.

observe the NiV G-specific cellular immune responses in both NiV G-ferritin and NiV sG immunized groups (Supplementary Fig. 1a, b), probably due to the sensitivity of the detection method we used, or NiV G head protein predominantly induced humoral immune responses as soluble form or in the context of the nanoparticle.

At three weeks post the first and second immunizations (Days 21 and 42), the NiV-binding IgG and pseudovirus-neutralizing titers were around 4- to 26-fold higher in mice immunized with 10 μg than 1 μg of NiV sG (Fig. 2b–e). Whereas for the NiV G-ferritin immunization groups, higher levels of serum NiV-binding IgG and pseudovirus-neutralizing titers in 10 μg group were only seen after the first dose (Days 7, 14, and 21), but antibody response augmentation was not observed after the second and third immunization (Days 42 and 61). In addition, the third dose of NiV sG resulted in around 135- and 5-fold increases in NiV pseudovirus-neutralizing titers for 1 μg and 10 μg groups, respectively. In comparison, the neutralizing titers only enhanced ~3-fold after the third dose of NiV G-ferritin compared to the titers after the second dose. These results indicate that NiV G-ferritin nanoparticle enhances the antigen-specific IgG titers and the neutralizing potency and exhibits the properties of dose sparing and dose reduction compared to its soluble counterpart.

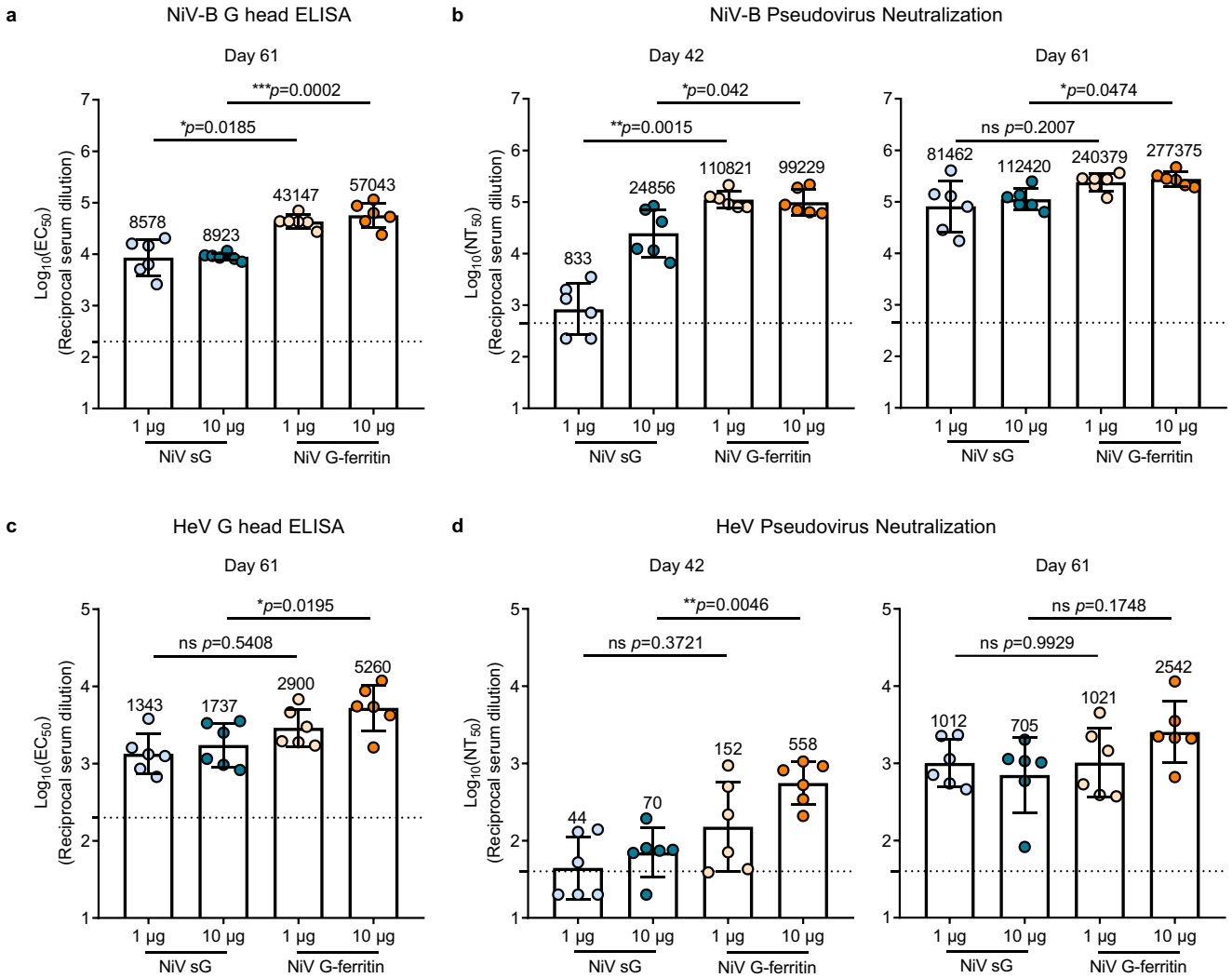

Fig. 3 | NiV G nanoparticle elicits cross-reactive neutralizing responses. a, **c** The serum cross-binding against recombinant NiV-B and HeV G head domain was measured by ELISA at Day 61 (~three weeks after the third immunization). The serum neutralizing titers against pseudotyped NiV-B (**b**) and HeV (**d**) at ~three weeks post the second (Day 42) and third (Day 61) immunizations were determined by pseudovirus neutralization assay. The numbers above the symbols indicate the geometric mean titers (GMTs). Dashed lines indicate the limit of detection (LOD) of the assays. The values lower than LOD were calculated as half of LOD. Experiments are performed in duplicate wells, and data from each group are shown as geometric mean with geometric SD. Statistical significance was determined by the one-way ANOVA with Tukey's multiple comparisons test. ns not significant, $^{*}p < 0.05$, $^{**}p < 0.01$, $^{***}p < 0.001$.

NiV G-ferritin induces broad antibody responses

We next tested the cross-reactivity of sera from immunized mice at Day 61 (~three weeks after the last immunization) against recombinant NiV-B, HeV, MojV, and LayV G head proteins by ELISA. The results showed that both the sera of NiV sG and NiV G-ferritin immunized mice could cross-bind to G head proteins of NiV-B and HeV. NiV G-ferritin induced higher cross-binding IgG titers to NiV-B and HeV G head proteins than NiV sG, although statistical significance in 1 μg groups against HeV G was not attained (Fig. 3a, c). In addition, the serum cross-reactive IgG titers against NiV-B were higher than those of HeV (Foldchange: ~5- to 15-fold), possibly due to NiV-B being more closely related to NiV-M than HeV. For MojV and LayV, no cross-binding antibody response was detected in sera of immunized mice (Supplementary Fig. 2a, b).

Cross-neutralizing potency against NiV-B and HeV was investigated using a VSV-based pseudovirus neutralization assay[46]. Immunization with NiV sG induced cross-pseudovirus neutralization against NiV-B after the second immunization (Day 42), and the neutralizing potencies improved ~100-fold and 5-fold for 1 μg and 10 μg groups following the third immunization (Day 61), respectively (Fig. 3b). In contrast, sera from NiV G-ferritin mice demonstrated ~133-fold (1 μg groups) and ~4-fold (10 μg groups) more robust cross-inhibitory activity against NiV-B after the second immunization (Day 42) than NiV sG groups, and only slight cross-neutralizing titer enhancement (< 3-fold for 1 μg and 10 μg groups) was observed following the third immunization (Day 61) (Fig. 3b).

Sera from vaccinated mice could also cross-neutralize HeV, although the cross-neutralizing titers against NiV-B were much higher than HeV (Fig. 3b, d). In addition, the cross-neutralization antibody titers to HeV after the third immunization were higher than those of the two immunizations for all vaccine immunization groups (Fig. 3d), indicating that increasing immunization times helps improve the cross-neutralization of HeV. Notably, NiV G-ferritin induced ~3-fold (1 μg groups) and 8-fold (10 μg groups) higher HeV cross-neutralizing antibody titers than NiV sG at day 42 (3 weeks post the second dose) (Fig. 3d). These results suggest that displaying the NiV G head domain on ferritin nanoparticles enhances cross-neutralizing antibody responses against HeV and NiV-B.

NiV G-ferritin elicits robust and durable neutralizing antisera

To investigate the stability of NiV G-ferritin, we also included a commercial aluminum-containing adjuvant and tested the storage and maintenance of

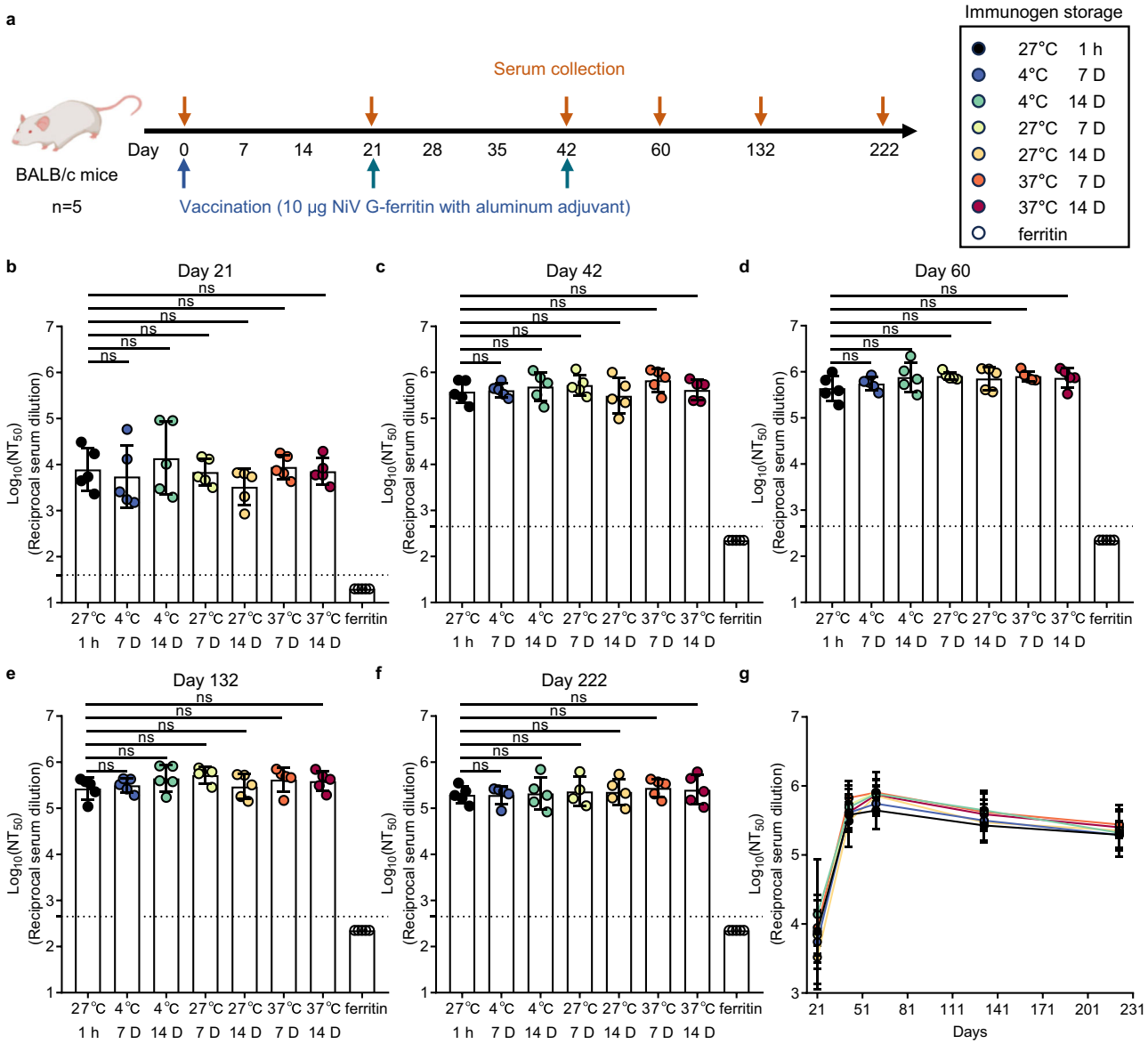

Fig. 4 | Stability and long-term efficacy of the NiV G nanoparticle vaccine. a The immunization schedule diagram. The NiV G-ferritin was first emulsified with an aluminum adjuvant and then stored at 4 °C, 27 °C, and 37 °C for 7 or 14 days, respectively. 6–8 weeks old mice were immunized with the above prepared NiV G-ferritin immunogens (corresponding to 10 μg NiV sG), and sera were collected at Days 21, 42, 60, 132, and 222 following first immunization for humoral immune response analysis. NiV G-ferritin vaccine stored at 27 °C for 1 h and ferritin alone were included as the positive or negative controls. **b**–**f** Serum neutralization titers against NiV-M pseudovirus and NT_{50} values are determined. Dashed lines indicate the limit of detection (LOD) of the assays. **g** Kinetics of NT_{50} titers after immunization with NiV G nanoparticle vaccine. Two independent experiments were performed in duplicate, and representative data are shown. Data from each group are shown as geometric mean with geometric SD. Statistical significance was determined by the one-way ANOVA with Dunnett's multiple comparisons test, compared with 27 °C 1 h group in **b**–**f**. ns not significant, $p > 0.05$.

NiV G-ferritin. We prepared NiV G-ferritin only or with AddaVax (NiV G-ferritin-AddaVax) or aluminum adjuvant (NiV G-ferritin-alum) and stored them at 4 °C, 27 °C, or 37 °C for varying time points (from 1 h to 14 days), and the stability of these samples was evaluated by SDS-PAGE, ELISA, and biolayer interferometry (BLI). We observed similar sizes and amounts of protein bands on the SDS-PAGE compared to correlated samples kept at 27 °C for 1 h or −80 °C (Supplementary Fig. 3a). Furthermore, all tested samples exhibited comparable binding signals to anti-NiV G mAbs (HENV-26 and nAH1.3) as determined by ELISA and BLI across all temperatures and storage periods (Supplementary Fig. 3b–e), suggesting that NiV G-ferritin alone or NiV G-ferritin with AddaVax or alum adjuvant are stable even after storage at 37 °C for 2 weeks.

Given the safety profile of aluminum adjuvant, we also examined the immunogenicity of aluminum-adjuvanted NiV G-ferritin (NiV G-ferritin-alum) and assessed the antibody responses in immunized mice (Fig. 4a). Consistent with AddaVax-adjuvanted NiV G-ferritin results, two-dose immunization with NiV G-ferritin-alum displayed equivalent neutralizing titers as three-dose immunization, which showed strong neutralizing potency with NT_{50} values > $10^{5.6}$ (for all vaccine groups at Day 60). The pseudovirus neutralization experiments showed that the NiV G-ferritin-alum induced a comparable humoral immune response at all tested conditions (Fig. 4b–g).

To assess the humoral immune response durability of the NiV G-ferritin-alum, we collected sera of the indicated groups at around three weeks (Day 60), three months (Day 132), and six months (Day 222) after the third immunization and measured pseudovirus-neutralizing antibody titers. The results showed that the sera of mice in all immunization groups maintained high pseudovirus-neutralizing antibody titers (NT_{50} > $10^{5.2}$) at

least six months after the third immunization (Fig. 4g), indicating that the NiV G-ferritin-alum could induce a long-lasting and robust humoral immune response even after storage for two weeks at 37 °C. These results indicate that NiV G-ferritin can endure room temperature transfer and storage for at least two weeks without compromised immunogenicity effect. As expected, ferritin-alum failed to induce pseudovirus-neutralizing antibodies against NiV-M.

Isolation and identification of NiV G-specific neutralizing mAbs

Since NiV G-ferritin can induce an excellent humoral immune response, we also isolated and characterized monoclonal antibodies (mAbs) from the spleens or lymph nodes of mice immunized with NiV G-ferritin. 27 anti-NiV G mAbs were generated with varying pseudovirus-neutralization activities. Recent works have identified several anti-NiV G monoclonal antibodies (HENV-32, HENV-26, nAH1.3, m102.3, and m102.4) with great neutralizing potency and structurally defined binding footprints on NiV G or HeV G proteins[43,47,48]. As m102.3 and m102.4 bound overlapped sites with the mAb HENV-26, we included HENV-32, HENV-26, and nAH1.3, representing all reported epitopes for comparison. Importantly, among the 27 mAbs, 24 mAbs inhibit NiV-M pseudovirus infection more potently than HENV-32, and 5 mAbs displayed higher neutralizing activity than all three published antibodies (HENV-32, HENV-26, and nAH1.3) (Fig. 5a).

To determine whether these 27 mAbs target different antigenic regions on the surface of NiV G head domain, we performed a competition binding assay using Bio-Layer Interferometry (BLI). The BLI assay showed that our mAbs can be classified into at least four competition-binding groups, among which group 1 and 2 antibodies (3 mAbs in group 1, and 1 mAb in group 2) recognize new antigenic sites differing from the three reported mAbs (Fig. 5b, c). Group 3 antibodies, including 7 mAbs, compete for NiV G binding with the human mAb HENV-26, which targets the receptor (ephrinB2) binding site of NiV G; and group 4 antibodies, including 16 mAbs, compete with the mouse mAb nAH1.3, which recognizes an epitope on the NiV G distal from the receptor binding site (Fig. 5b). Interestingly, we did not isolate mAbs that compete for the G binding with the mAb HENV-32 (group 5), a human mAb that binds an epitope distinct from HENV-26 and nAH1.3.

NiV G immunogens elicited antisera target four distinct epitopes

Next, we investigated the antibody composition in sera from mice immunized with NiV sG and NiV G-ferritin by serum competition ELISA assay. We selected representative mAbs from five competition groups (S1E2, S2B10, LN3A12, LN3D3, and HENV-32, respectively) and compared the binding signals of these five mAbs to the NiV G protein in the presence or absence of mouse serums. The results showed that NiV sG and NiV G-ferritin could induce antibodies that compete for NiV G binding with mAbs in groups 1–4, and no significant serum blockade effect was observed for mAb in group 5. These results indicate that sera recognize at least four dominant antigenic sites on the NiV G-head protein, illustrating the diversity of polyclonal antibody responses induced by NiV G antigen (Fig. 6a). For group 2 and 4 antibodies competition, NiV G-ferritin and NiV sG immunized mouse sera displayed comparable effects. However, for groups 1 and 3 antibodies competition, the NiV G-ferritin group revealed stronger blockade activity than the NiV sG group, indicating that NiV G-ferritin likely induced higher concentrations or binding affinities of groups 1 and 3 antibodies than NiV sG (Fig. 6a).

We further quantitatively evaluated the proportion of distinct antibodies in the sera of immunized mice. In this setting, immobilized G protein was first incubated with excess mAbs from different groups, or non-G-binding isotype control mAb, or blocking buffer without any mAbs. Then, the binding signals of antisera from immunized mice were monitored. We found that antibodies recognizing the receptor-binding site contribute the most to the NiV G-binding IgG (~50%) in sera from mice immunized with either NiV sG or NiV G-ferritin (Fig. 6b). In addition, group 5 antibodies have not been detected in all immunized mouse sera (Fig. 6b), which is in line with the serum competition results (Fig. 6a).

NiV G-ferritin completely protects Syrian golden hamsters from the lethal NiV-M challenge

We next used a Syrian golden hamster model to investigate whether the immune responses induced by NiV G-ferritin have protective activity against the homologous NiV-M challenge. As the body weight of six-week-old hamster is higher than that of six-week-old mice (~5-fold), we first used 2-fold higher amounts of antigen in the hamster vaccination study. The hamsters were immunized with different amounts of NiV G-ferritin and NiV sG (2, 6, and 20 μg/dose, $n = 3$) twice, then the serum neutralizing antibody titers against NiV-M pseudovirus were investigated (Supplementary Fig. 4). The neutralizing antibody titers in hamsters receiving NiV G-ferritin were observed after the first (Day 21) and the second (Day 39) immunizations, and we found similar neutralizing activities in the 2 μg group compared to the higher dose groups (6 μg/dose and 20 μg/dose) (Supplementary Fig. 4c, d). In addition, the NiV-M pseudovirus-neutralizing titers in hamsters receiving NiV sG were below the detection level after the first immunization at all three tested amounts, and only varied neutralizing activities in the NiV sG groups were observed after the second immunization. When vaccinated hamsters were challenged with lethal NiV-M infection three weeks after the second dose, all NiV G-ferritin immunized hamsters were protected from mortality without weight loss (Supplementary Fig. 4e, f). In comparison, one hamster injected with 20 μg/dose of NiV sG died at day 6 post NiV-M challenge.

Since 2 μg/dose of NiV G-ferritin induced protective activity against NiV-M challenge in hamsters, but two doses of NiV sG likely not confer 100% protection, we further investigated the protective efficacy of NiV sG and NiV G-ferritin in a three-dose immunization schedule. Hamsters were immunized three times with 2 μg/dose of NiV sG, equimolar NiV G-ferritin, or ferritin, and the hamster sera were collected three weeks after each vaccination (Fig. 7a). The results of the pseudovirus neutralization experiments showed that NiV G-ferritin rapidly induced detectable neutralizing titers (geometric mean NT_{50}, 1:1204) against NiV-M pseudovirus after the first immunization (Fig. 7b). In contrast, after the second immunization, NiV sG induced a relatively weaker pseudovirus-neutralizing titer (NT_{50}, 1:584) in hamsters (Fig. 7b). With the progress of the second and third immunizations, hamster serum pseudovirus-neutralizing titers induced by NiV G-ferritin and NiV sG increased (Fold change of NT_{50} values between the second and third immunizations: 4.2-fold for NiV G-ferritin group, and 14.4-fold for NiV sG group). Consistently, the NiV G-ferritin immunized hamster sera after the third immunization showed ~2-fold increased neutralizing potency against two authentic NiV viruses than NiV sG group, and no neutralizing antibody was detected in the hamster serums immunized with ferritin alone (Fig. 7c). These results are consistent with the humoral immunity results in mice, although the neutralizing potency of hamster sera is considerably weaker than mouse sera (Fig. 2).

Three weeks after the third immunization, all experimental hamsters were injected intraperitoneally with a lethal dose of NiV-M (1000 LD_{50}) (Fig. 7a). The survival rates were monitored 21 days after the challenge ($n = 6$ per group). All vaccine-immunized hamsters survived the lethal challenge during the 21 days of observation without significant weight loss observed. All the control animals immunized with ferritin died within 6 days after the NiV-M challenge (Fig. 7e, f). Six of the hamsters in each group were euthanized on Day 5 after the virus infection, and the lungs, brains, and spleens were harvested for viral load detection. Viral titers were measured using real-time PCR (qRT-PCR). High levels of NiV RNA were detected in the euthanized hamsters' lungs (mean value: ~$10^{9.7}$ copies/g), brains (mean value: ~$10^{7.9}$ copies/g), and spleens (mean value: ~$10^{9.4}$ copies/g) in the ferritin control group, while no NiV RNA was detected in the vaccine groups (Fig. 7g), suggesting that three doses of NiV G-ferritin and NiV sG completely diminished viral replication in lungs, brains, and spleens, and protected hamsters against the lethal NiV challenge.

Discussion

As a re-emerging zoonotic virus characterized by a high fatality rate, NiV possesses the potential to instigate significant epidemics in humans[49]. Although various NiV vaccine candidates have undergone testing in the

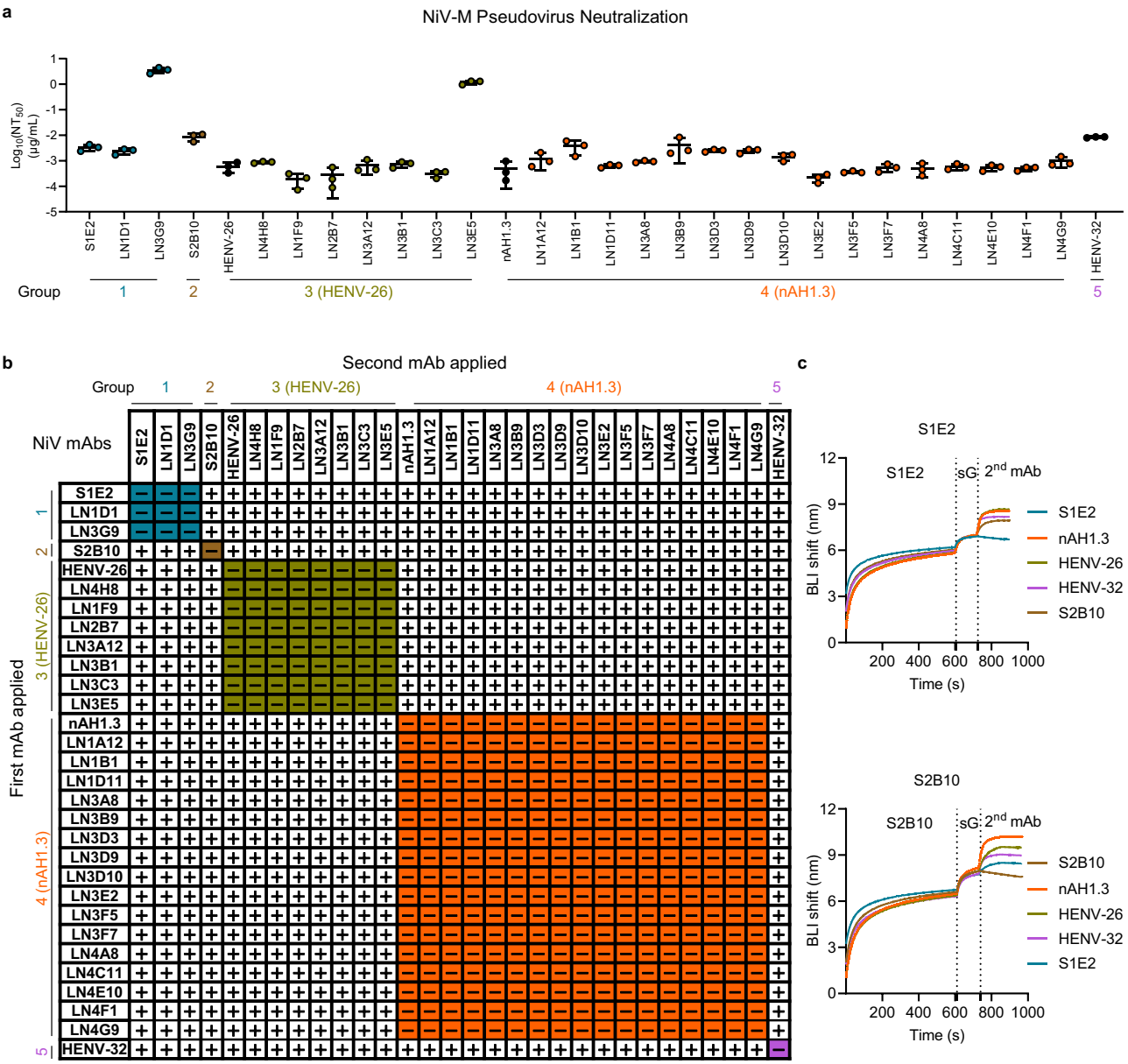

Fig. 5 | Profile of NiV G-specific mAbs isolated from NiV G nanoparticle-immunized mice. a 27 NiV G-binding mAbs were generated from NiV G-ferritin immunized mice, and the neutralizing potency of these mAbs against NiV-M was determined using a NiV pseudovirus neutralization assay. Data shows the mean and SD from three independent experiments performed in duplicate. **b** The competition binding assay among isolated NiV G mAbs for binding to NiV sG protein was measured by biolayer interferometry (BLI). The 27 NiV G mAbs were grouped into four classes. The indicated mAb in the column was first loaded onto protein A biosensors; then, the biosensors were dipped into a buffer with NiV sG protein, followed by immersion into the buffer containing the second mAb. An increasing BLI signal when the addition of the second mAb indicates an unoccupied epitope (non-competitor, shown "+" in the table), whereas no binding indicates epitope blocking (competition, shown "−" in the table). HENV-26, HENV-32, and nAH1.3 are previously reported mAbs that target distinct epitopes on NiV G. The results represent two independent experiments. **c** Representative competition binding BLI curves of S1E2 and S2B10.

preclinical and clinical phases, there is still no FDA-approved NiV vaccine or effective treatment for NiV disease[4]. Thus, the imperative to develop additional safe, effective, and low-cost NiV vaccines remains crucial. Previous studies showed that NiV G protein is an essential antigen for vaccine development[23–25], especially the head domain of G protein, which exhibits unique immune advantages over the ectodomain of G protein[47]. Here, we designed a NiV G head domain-based nanoparticle immunogen and thoroughly characterized the immune responses in mice and hamsters. In addition, we isolated a panel of mAbs with varying neutralizing activities that recognize four distinct antigenic sites on NiV G protein.

Although subunit vaccines are regarded as the safest among various vaccine platforms, traditional recombinant subunit vaccines exhibit apparent drawbacks[50,51]. Compared with conventional subunit vaccines, self-assembling nanoparticle vaccines share some features as VLPs and likely confer more robust immune responses in vivo, which is possible due to (1) repetitive antigen structures conferring high avidity binding of nanoparticle to low-affinity B cells; (2) the larger size of nanoparticle altering antigen trafficking, accumulation, and processing by immune cells and systems. Although soluble NiV sG could induce neutralizing antisera in both mice and hamsters, the binding and neutralizing titers elicited by NiV

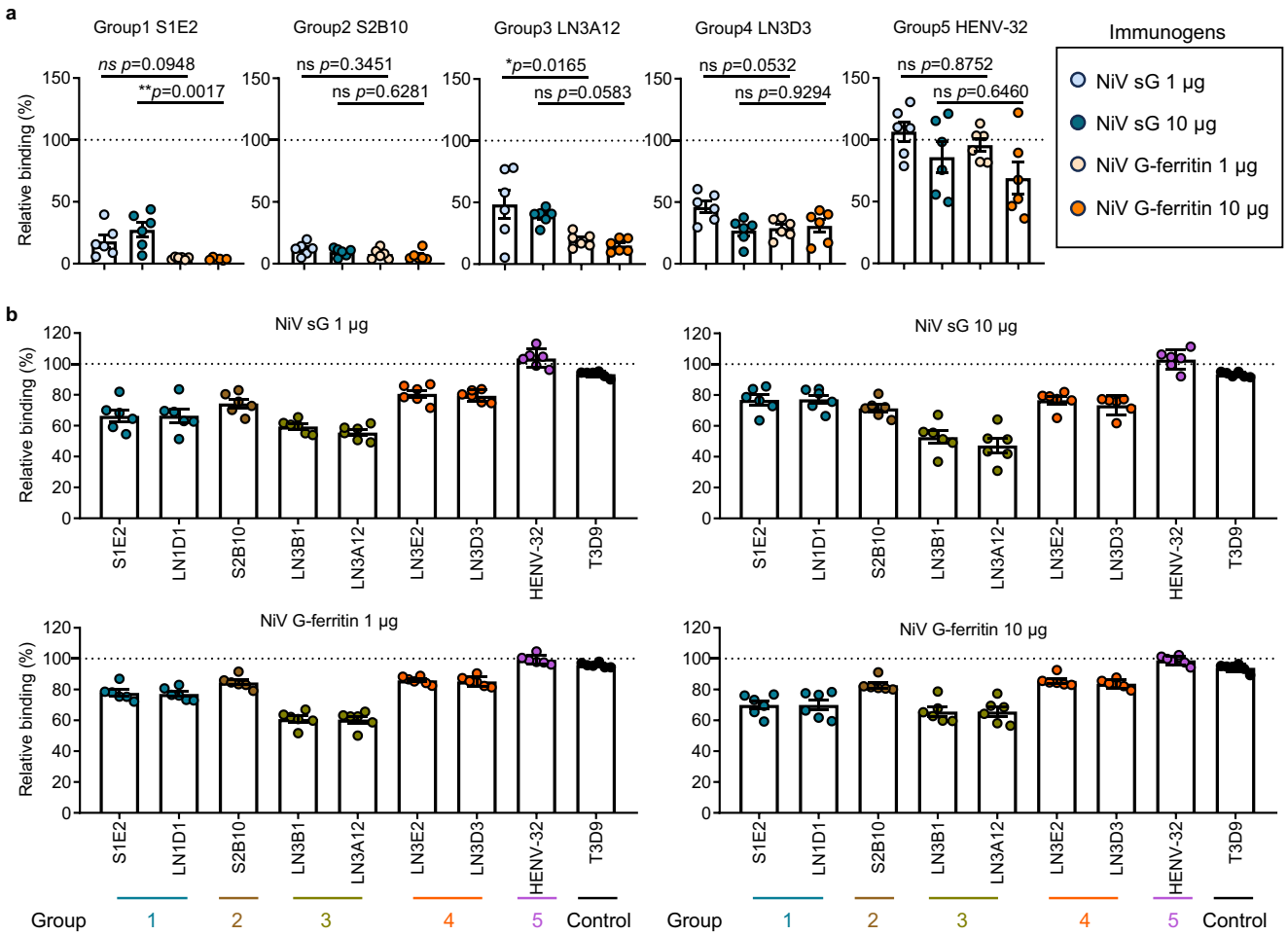

Fig. 6 | NiV G-specific mAbs proportion and quantification in sera of vaccinated mice. a A competition ELISA showing binding of S1E2 (group 1), S2B10 (group 2), LN3A12 (group 3), LN3D3 (group 4), and HENV-32 (group 5) mAbs to the immobilized NiV sG protein in the presence of 100-fold dilution vaccine-elicited mouse sera (obtained at Day 61, ~three weeks after the third immunization). The binding of these mAbs without vaccine-elicited mouse sera was used as a control, and the OD450 (absorbance at 450 nm) value was defined as 100%. **b** Quantification of the proportion of different group antibodies in sera from vaccinated mice. ELISA showing binding of NiV sG or NiV G-ferritin vaccinated mouse sera (20000-fold dilution) to the immobilized NiV sG protein in the presence of 10 μg/mL group 1 (S1E2 and LN1D1), group 2 (S2B10), group 3 (LN3A12 and LN3D3), group 4 (LN3E2 and LN3D3) or HENV-32 mAbs. The anti-SFTSV mAb T3D9 was used as a control (not published). Two independent experiments were performed in duplicate, and representative results are shown. Data in each group are presented as mean ± SEM. Statistical significance was determined by the one-way ANOVA with Tukey's multiple comparisons test. ns not significant, $*p < 0.05$, $**p < 0.01$.

G-ferritin were more robust and potent. While some nanoparticle vaccines could also trigger cellular immunity[37,52], we did not observe a cellular response in NiV G-ferritin or NiV sG immunized mice. This might be due to the different antigens, nanoparticle scaffolds, immunization doses, or animal models used in the experiments. Like our NiV G-ferritin, several nanoparticle vaccines also predominantly induce a humoral immune response, as seen for nanoparticle vaccines against Lassa virus[53], SARS-CoV-2[54], influenza virus[35], respiratory syncytial virus[55] and Powassan virus[56].

Despite the differences in humoral responses, three immunizations with NiV G-ferritin and NiV sG completely protected against lethal NiV challenge in hamsters with no evidence of viral RNA in tissues collected from immunized animals. Additionally, two doses of NiV G-ferritin also conferred complete protection against lethal NiV-M challenges with continuous body weight gain observed (Supplementary Fig. 4), but one of three hamsters immunized with 20 μg/dose of NiV sG succumbed to NiV infection (Supplementary Fig. 4e). These results indicate that the protective efficacy of NiV G-ferritin seems to be equivalent to or, in some contexts, better than that of NiV sG in a three- or two-dose immunization regimen. Since a single NiV G-ferritin immunization elicited robust pseudovirus-neutralizing antibodies in both mice and hamsters, we speculate that a single vaccination may also confer protection against lethal NiV challenge in animals, although this requires further investigation.

Additionally, the hamsters did not lose body weight (Fig. 7d and Supplementary Fig. 4b) or show noticeable adverse events during the immunization period, indicating that safety may not be a concern. We also assessed the protein stability and immunogenicity of NiV G-ferritin under various storage temperatures and found that NiV G-ferritin is stable for at least two weeks, with temperatures even higher than standard room temperature. This diminishes the requirement for cold chain transportation encountered with other vaccines. Noteworthy, our nanoparticle vaccine is generated by genetically fused NiV G head domain to ferritin and expressed using a eukaryotic expression system, which eliminates the need for separate steps of protein purification and in vitro assembly of antigen with nanoparticle scaffolds, greatly favored vaccine safety and a more streamlined production process.

Recent studies have shown that isolated neutralizing mAbs can provide in vivo protection against NiV infection. NiV G-ferritin exhibits excellent immunogenicity with potent cross-neutralizing activities against NiV-B and HeV, promoting us to isolate mAbs from NiV G-ferritin immunized mice. A panel of 27 mAbs was identified, and these mAbs recognize non-overlapping antigenic sites on NiV G protein.

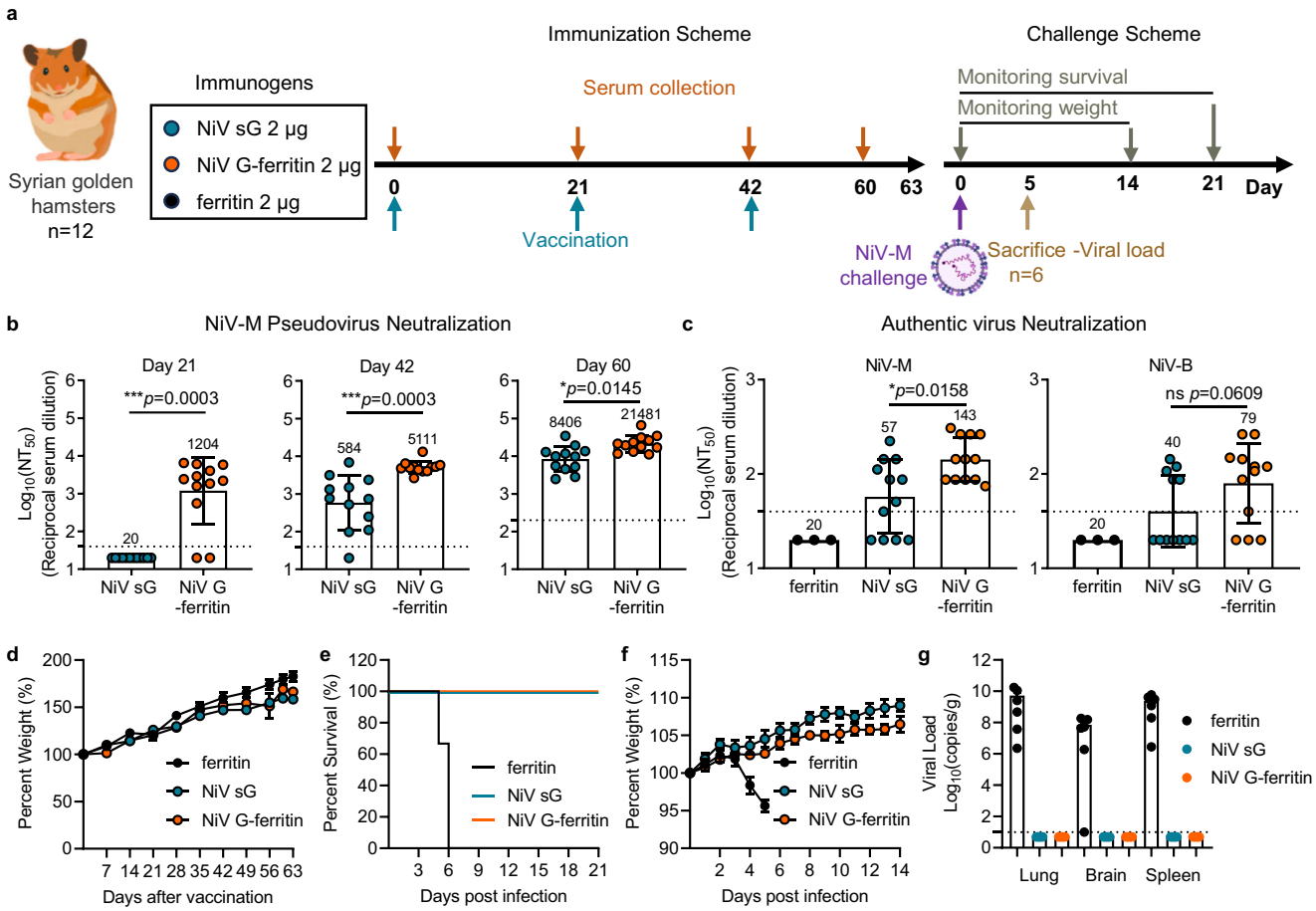

Fig. 7 | NiV G-ferritin protected Syrian golden hamsters from the lethal NiV Malaysia challenge. a The experimental scheme of Syrian hamsters. The animals ($n = 12$) were intramuscularly vaccinated with three doses of either 2 μg NiV sG, equivalent NiV G-ferritin, or ferritin mixed 1:1 with the AddaVax adjuvant at a three-week interval and then challenged with the NiV Malaysia strains at 1000 LD_{50} via the i.p. route. **b** NiV-M pseudovirus neutralization titers at Day 21 (three weeks after the first immunization), Day 42 (three weeks after the second immunization), and Day 60 (~three weeks after the third immunization) for antisera from individual hamsters. Two independent experiments were performed in duplicate, and representative results are shown. **c** Neutralization titers against two authentic NiV strains (NiV-M and NiV-B) at Day 60. **d** Weight change of Syrian hamsters during the immunization scheme. Survival (**e**), and weight change (**f**) of Syrian hamsters challenged with the NiV Malaysia strain. **g** Viral loads in the hamster lungs, brains, and spleens at 5 dpi were measured by quantitative PCR with reverse transcription (qRT-PCR). Data in each group are presented as geometric mean with geometric SD in **b** and **c** and mean ± SEM in **f** and **g**. Dashed lines indicate the limit of detection (LOD) of the assays. The values lower than LOD were calculated as half of LOD. Two-tailed, unpaired t-tests determined statistical significance. ns not significant, $^{*}p < 0.05$, $^{***}p < 0.001$.

They also exhibited highly potent in vitro neutralization activities against NiV pseudovirus infection, offering an excellent opportunity for mAb cocktail treatment in the future.

In sum, we successfully designed a NiV G nanoparticle vaccine candidate against NiV by using the head domain of NiV G protein as the antigen target and ferritin as the antigen display platform. We found that the NiV G head domain is an exemplary antigenic target for NiV vaccine development. Furthermore, potential therapeutic antibodies against NiV infection were isolated, providing attractive pipelines and strategies for mAb generation and immunogenicity evaluation. Given that NiV G-ferritin elicits strong and protective humoral immunity in mice and hamsters, it deserves further evaluation.

Methods

Ethics statement

Animal experiments were approved by the Animal Ethics Committee of Wuhan University (WDSKY0202201) and the Wuhan Institute of Virology, Chinese Academy of Sciences (WIVAF21202301). The authentic virus infections were performed in the animal biosafety level 4 (ABSL-4) facility at the National Biosafety Laboratory (Wuhan), Chinese Academy of Sciences.

Viruses and cells

The NiV Malaysia (AF212302.2) and NiV Bangladesh (AY988601.1) strains used in the authentic virus neutralization assay and the challenge studies were obtained from the National Virus Resource Center, Wuhan Institute of Virology, Chinese Academy of Sciences. All authentic viruses were propagated in Vero E6 cells. Vero E6 or 293 T cells were maintained in DMEM (Monad Biotech) with 8% or 10% heat-inactivated FBS (ExCell Bio) at 37 °C with 5% CO_2.

Cloning, protein expression, and purification

The genes encoding G (NP_112027.1) and F (NP_112026.1) of NiV-M, G (AAY43916.1) and F (AAY43915.1) of NiV-B, G (NP_047112.2) and F (NP_047111.2) of HeV, G (YP_009094095.1) of MojV, G (UUV47206.1) of LayV, *Helicobacter pylori* ferritin (WP_000949190.1) and bullfrog ferritin fragment (ESQVRQQF) were codon optimized and synthesized by Tsingke Biotechnology Co. Genes encoding the full-length G and F of NiV-M, NiV-B, and HeV were cloned into a mammalian expression vector respectively for pseudovirus generation. The gene encoding *Helicobacter pylori*-bullfrog hybrid ferritin was constructed as previously described[38] and cloned into a mammalian expression vector with an N-terminal 6×His-tag without signal-peptide for protein production. The gene encoding NiV G-ferritin was constructed by fusing the C-terminal of the NiV G head domain with

the N-terminal extension of ferritin. Genes encoding NiV G-ferritin, NiV sG (residues:176–602), NiV-B G head domain (residues:176–602), HeV G head domain (residues:176–605), LayV G head domain (residues:176–625) and MojV G head domain (residues:176–625) were individually cloned into a mammalian expression vector with an N-terminal 6×His-tag and signal peptide for protein production. All plasmids were verified by DNA sequencing.

For protein purification, the above expression vectors were transiently transfected into Expi293F cells with Polyethylenimine (PEI, Polysciences), and the supernatants of cultured cells (except the cells transfected ferritin) were harvested 108 h after transfection. The supernatants were filtered through a 0.45 μm filter, and the recombinant proteins were purified by Ni-Charged Resin (GenScript). For ferritin purification, the transfected Expi293F cells were harvested 108 h post-transfection, resuspended in the lysis buffer (50 mM Tris-HCl pH 7.5, 100 mM NaCl, 0.25% NP-40, and 100 μg/mL PMSF) and broken with a Dounce grinder. Then, the cell lysate was centrifuged at 12,000 × *g* for 40 min to remove cell debris. The supernatant containing ferritin protein was filtered through a 0.45 μm filter and then purified by Ni-TED resin (GenScript). The proteins above were further purified by size-exclusion chromatography (SEC) using Superose 6 Increase 10/300 GL column (Cytiva) or Superdex 200 Increase 10/300 GL column (Cytiva).

Negative stain electron microscopy

Purified nanoparticles were serially diluted to 800/400/200/100/50 nM, and 10 μL samples were then adsorbed onto a 300-mesh copper grid (Beijing Daji Keyi Technology Co., Ltd, D11023) for 1 min. Then, the excess solution was blotted away with filter paper. The grids were stained with 2% uranyl acetate for 30 s, and the excess solution was blotted away. Images were collected using a transmission electron microscope (JEOL, JEM-1400plus) or a Talos L120C (Thermo Scientific) electron microscope.

Dynamic light scattering (DLS)

Proteins were filtered by a 0.22 μm filter and diluted to approximately 0.5 mg/mL using a buffer containing 20 mM Tris-HCl pH 8.0 and 150 mM NaCl. Then, the samples were loaded into a microcuvette to measure the hydrodynamic diameters and polydispersity using the Zetasizer Nano ZSP instrument (Malvern Panalytical). Each sample was performed triplicate measurements, and each parallel repeat lasted 60 s at 25 °C. The hydrodynamic diameters and polydispersity index of the samples were analyzed using instrument software (Malvern Panalytical).

Differential scanning fluorimetry (DSF)

The thermostability of target proteins was determined using a PSA-16 instrument (BEST Science & Technology, Beijing, China). The sample was diluted to 0.5 mg/mL, and 20 μL of diluted sample was loaded into a quartz glass tube (Cat#LG-002, BEST Science & Technology, Beijing, China). The intensity of the intrinsic protein fluorescence at 330 and 350 nm was measured using a linear temperature scan from 23 to 97 °C at a heating rate of 1 °C/min. The thermal transition midpoint (Tm) was calculated based on the slope of the F350/F330 curve. Each sample was measured four times.

Size exclusion chromatography coupled with multi-angle light scattering (SEC-MALS)

A 100 μL volume of each sample (0.5 mg/mL for NiV G-ferritin and 2 mg/mL for NiV sG) was injected onto the WTC-030S5 column (Wyatt Technology, Santa Barbara, CA, USA) with an isocratic run at 0.5 mL/min for 40 min. 20 mM Tris-HCl pH 8.0 and 150 mM NaCl were used as the mobile phase. A MALS detector (DAWN®) and a refractive index (RI) detector (Wyatt Technology, Santa Barbara, CA, USA) were connected in series to the UV detector on the SEC system. Bovine Serum Albumin (BSA, Thermo Scientific) was used to normalize the static light scattering detector. The light scattering, differential refractive index (dRI) measurements, and molecular weights were analyzed using ASTRA software (6.1.2.84) (Wyatt Technology, Santa Barbara, CA, USA).

Enzyme-linked immunosorbent assay (ELISA)

The antigenicity of NiV G-ferritin was measured by ELISA. Briefly, 96-well ELISA plates (Corning) were coated overnight at 4 °C with 3 μg/mL of NiV sG or NiV G-ferritin in coating buffer (0.1 M carbonate, pH 9.6). After four times washes with PBS-T (PBS with 0.05% Tween 20), all wells were blocked with 50 μL of blocking buffer (1% BSA in PBS-T) for 2 h at 37 °C. After blocking, NiV G mAbs HENV-32, HENV-26, nAH1.3, and anti-Rabies virus mAb RVC20 (a negative control) were serially diluted from 5 μg/mL and then added to the plates and incubated at 37 °C for 2 h. Plates were washed four times in PBS-T before adding HRP conjugated goat anti-human IgG (1 : 20000 dilution, ABclonal, AS002) for 1 h at 37 °C. Plates were washed and colored with 50 μL/well of one component TMB chromogen solution (NCM Biotech) for 10–30 min at 37 °C. Substrate reactions were stopped by adding 50 μL/well of 1 M HCl, and the absorbance was measured at 450 nm (OD450). For the serum binding titer detection, we performed a similar procedure, and G head proteins of NiV-M, NiV-B, HeV, LayV, and MojV were coated on the ELISA plates, and HRP conjugated goat anti-mouse IgG (1 : 8000 dilution, ABclonal, AS003) was used.

Animal experiments-BALB/c mice

BALB/c mice (6–8 weeks old, female) were purchased from Vital River Laboratories (Beijing, China). For the vaccine immunogenicity assessment experiment, BALB/c mice were randomly allocated into six groups, with each group containing six mice. Mice were vaccinated with 1 μg or 10 μg of NiV sG or corresponding amounts of NiV G-ferritin containing an equimolar ratio of NiV sG. Control group mice were immunized with PBS or equimolar (compared to 10 μg NiV sG) ferritin. All the mice were vaccinated three times via the intramuscular (i.m.) route with the AddaVax adjuvant (InvivoGen) and injection interval of three weeks. Sera were collected at different times (Days 7, 14, 21, 42, and 61 after the first immunization) to detect humoral immune responses. On Day 61, mice were sacrificed by the cervical dislocation after being anesthetized by 2% isoflurane, and splenocytes and lymph node cells were harvested for cellular immune response analysis and antigen-specific B cell sorting.

For the temperature stability assay, BALB/c mice were randomly allocated into nine groups with each group containing five mice. NiV G-ferritin vaccine was prepared by mixing NiV G-ferritin with Imject Alum adjuvant (Thermo Scientific). Then, the prepared NiV G-ferritin-alum vaccine was stored at 4 °C, 27 °C, and 37 °C for 7 or 14 days, respectively. The sample of NiV G-ferritin-alum stored at 27 °C for 1 h served as a positive control, and mice immunized with PBS or equimolar ferritin were negative controls. All the mice were vaccinated three times via the i.m. route with an interval of three weeks. Sera were collected at predetermined times to detect humoral immune responses.

Animal experiments-Syrian hamsters

Syrian hamsters (six weeks old, female) were purchased from Vital River Laboratories (Beijing, China) and randomly divided into three groups, with each group containing 12 animals. 2 μg of NiV sG, NiV G-ferritin (containing equivalent 2 μg of NiV G antigen), or equimolar ferritin was adjuvanted with 50% (volume ratio) AddaVax adjuvant (InvivoGen). Then, these immunogens were intramuscularly administrated to hamsters three times at a three-week interval. Serum samples were collected and subjected to immunological assays at the indicated time points. Three weeks after the final immunization, all animals were transferred to the ABSL-4, and each hamster was challenged with 1000 LD_{50} NiV-M via the intraperitoneal injection route. Before vaccination, retro-orbital bleeding and virus inoculation, hamsters were anesthetized with 5% isoflurane. Half of the animals in each group were euthanized by cervical dislocation under isoflurane anesthesia five days after being challenged with NiV-M, and the organs of the lung, brain, and spleen were harvested for viral load detection through qRT-PCR. The other half of the animals in each group were monitored for 21 days after the challenge, and the survival rate was calculated at the end of the monitoring time. The weight change was monitored daily for 14 days.

In the two-dose immunization regimen, hamsters were randomly divided into eight groups, with each group containing three animals. The hamsters were vaccinated with 2 μg, 6 μg, or 20 μg NiV sG, or equimolar NiV G-ferritin mixed with AddaVax adjuvant (1:1 volume ratio) twice with a three-week interval, respectively. Control group hamsters were immunized with PBS or equimolar (compared to 20 μg NiV sG) ferritin. Three weeks after the second immunization, all animals were transferred to the ABSL-4, and each was challenged with 1000 LD_{50} NiV-M via the i.p. route. The hamsters were monitored for weight change and survival rate for 21 days after the NiV-M challenge.

During the experiments, all hamsters were acclimated to the Specific Pathogen Free (SPF) barrier environment for at least one week prior to the experiment. They were euthanized by cervical dislocation under isoflurane anesthesia if they experienced more than 25% weight loss after the challenge or at the end of the experiment. Animal immunization and challenge experiments do not allow for blinding. The individual who performed the tissue sample analysis did not know the identity of the samples.

Pseudovirus neutralization assay

NiV-M, NiV-B, or HeV full-length F and G glycoproteins were pseudotyped using VSVΔG-eGFP, a reporter virus in which the VSV-G glycoprotein has been replaced with an eGFP reporter gene. To increase the NiV-B pseudovirus titer, we introduced S207L and G252D point mutations on the NiV-B F protein. For the pseudovirus production, 293 T cells were transiently transfected to overexpress F and G glycoproteins. 24 h after transfection, the cells were infected with VSVΔG-eGFP for 4–6 h and then washed with PBS and incubated with 1 μg/mL of anti-VSV G monoclonal antibody-I1[57]. 24 h post infection, supernatants were collected and centrifuged at 1500 × *g* for 5 min to remove the cell debris and aliquoted appropriately before storage at −80 °C to avoid multiple freeze thaws.

For the pseudovirus neutralization assay, serum samples were heat-inactivated at 56 °C for 30 min before experiments. Pseudovirus was diluted and mixed with serial dilutions of sera/mAbs in 96-well plates and incubated for 1 h at 37 °C. The virus-serum/mAb mixtures were added to Vero E6 cells seeded at a density of 1.5×10^4 cells/well in the 96-well plates the day before. 24 h later, the cells were fixed with 4% paraformaldehyde, and then the green fluorescent dots (GFP signal) were counted and analyzed using CTL ImmunoSpot Analyzer (S6 Ultra M2, Cellular Technology) and ImmunoSpot Software (ImmunoSpot 7.0.34.0, Cellular Technology). Half-maximal inhibitory concentrations (NT_{50}) values were calculated from neutralization curves using a nonlinear regression model and plotted with GraphPad Prism (v.8.0).

Authentic virus neutralization assay

The virus stock was propagated in Vero E6 cells. The serum samples of mice and hamsters (sera were heat-inactivated for 30 min at 56 °C) were serially diluted starting from 1:40 dilution in DMEM containing 2% FBS and incubated with either 100 $TCID_{50}$ NiV-M or 50 $TCID_{50}$ NiV-B for 1 h at 37 °C. Virus and serum mixtures were added to Vero E6 cells at 37 °C with 5% CO_2 for 1 h, and the cytopathic effect in each well was calculated five days after infection. Four replicates were set for each serum dilution. NT_{50} values were calculated using IBM SPSS Statistics 27.

qRT-PCR

Five days after the challenge, the lungs, brains, and spleens of hamsters were collected after euthanasia to measure the viral RNA copies in the tissues. Each hamster tissue was homogenized in 1 mL DMEM in a tissue grinder, and the samples were inactivated before removal from the BSL-4 laboratory. The tissue homogenate supernatant was taken to RNA extraction using a Qiagen RNeasy Mini kit. RNA was analyzed using primers/probes targeting the NiV nucleocapsid (N) gene for quantitative real-time PCR (qRT-PCR), and the primers and probes were used as follows: forward primer (5'-AACATCAGCAGGAAGGCAAGA-3'), reverse prime (5'-GCCACTCTGTTCTATAGGTTCTTC-3'), probe (5'FAM-TTGCTGCAGGAGGTGTGCTC-BHQ1-3'). NiV RNA was detected using the CFX96 Real-Time system (Bio-Rad) in HiScript II One Step qRT-PCR Probe Kit (Vazyme). The standard curve was constructed with 9 points in a 20 μL reaction system (1×10^9 to 1×10^1 copies). Samples with fewer than ten copies were defined as negative.

Measurement of IFN-γ and IL-4 in spleen cell supernatant by ELISA

The production of IFN-γ and IL-4 in the cell culture supernatant was measured using IFN-γ/IL-4 Mouse Uncoated ELISA Kit (Invitrogen, 88-7314-88/88-7044-86). Briefly, the isolated splenocytes were diluted to 5×10^6 cells/mL with RPMI 1640, and then NiV sG was added to the cells at a final concentration of 5 μg/mL. Then, the mixtures were divided into 96-well plates. The cells stimulated with Cell Stimulation Cocktail (500×, eBioscience™, Invitrogen) were used as a positive control, and the cells incubated with 5 μg/mL BSA were used as a negative control. The plates were incubated at 37 °C with 5% CO_2 for 72 h, and then IFN-γ and IL-4 in the culture supernatants were determined using IFN-γ/IL-4 Mouse Uncoated ELISA Kit according to the manufacturer's protocol.

Intracellular cytokine staining assay

The isolated splenocytes were diluted to 5×10^6 cells/mL with RPMI 1640, and then 5 μg/mL NiV sG was added to the cells for the stimulation. The mixtures were divided into 6-well plates, and the cells stimulated with Cell Stimulation Cocktail (500×, eBioscience™, Invitrogen) were served as a positive control; the cells added with 5 μg/mL BSA were used as a negative control, with PBS-treated cells as blank control. The plates were incubated for 2 h in a cell incubator at 37 °C with 5% CO_2, and then Monensin Solution (1000×, eBioscience™, Invitrogen) was added to cells, and cells were cultured for another 4 h. After fixing with 4% paraformaldehyde and washing with PBS, the cells were stained with Ms CD4-BV510 (1 : 100 dilution, BD Pharmingen™, 563106), IFN-γ-PE (1 : 80 dilution, Invitrogen, 12-7311-82), IL4-APC (1 : 80 dilution, Invitrogen, 17-7041-82) or Ms CD8a-BV510 (1 : 100 dilution BD Pharmingen™, 563068), IFN-γ-PE, IL4-APC. The percentage of $IFN\text{-}\gamma^+/IL4^+$ cells was measured using CytoFLEX Flow Cytometer (Beckman). The data were processed using FlowJo software.

Isolation of NiV G-specific B cells and amplification of antibody variable region sequence

After 21 days of the third immunization, mice immunized with the NiV G nanoparticle were sacrificed, and splenocytes and lymph node cells were harvested for antigen-specific B cell sorting. Briefly, the NiV sG were randomly biotinylated with EZ-Link NHS-PEG4-Biotin (Thermo Scientific), and the isolated cells were stained with 0.5 μg/mL of biotinylated NiV sG for 30 min at 4 °C. After washing with PBS (1 mM EDTA, 2% FBS), the cells were stained with Fixable Viability Stain 780 (1 : 1000 dilution, FVS780, BD Biosciences, 565388), Ms CD3e-BV510 (1 : 100 dilution, BD Biosciences, 563024), Ms CD4-BV510 (1 : 100 dilution, BD Biosciences, 563106), Ms CD8a-BV510 (1 : 100 dilution, BD Biosciences, 563068), Ms CD19-PE-Cy7 (1 : 100 dilution, BD Biosciences, 552854), Ms IgD-PerCP-Cy5.5 (1 : 100 dilution, BD Biosciences, 564273), CD138-FITC-A (1 : 100 dilution, BD Biosciences, 564511), CD95-PE-A (1 : 100 dilution, BD Biosciences, 554258) and Streptavidin-APC (1 : 1000 dilution, BD Biosciences, 554067) for 30 min at 4 °C. After washing, the cells were loaded on FACS Aria III (BD Biosciences). The target cells (780^-, $CD3/4/8^-$, $CD19^+$, IgD^-, $CD95^+$, and NiV G^+) were sorted into 96-well PCR plates (Bio-Rad), with each well containing 7 μL of catch buffer (10 mM Tris-HCl, 1U/μL Rnain), and stored at −80 °C. NiV G-specific B cell genes were isolated following a previously published protocol[58].

Expression and purification of monoclonal antibodies

The paired heavy-chain and light-chain plasmids of antibodies at a molar ratio of 1:1.2 were transiently co-transfected into Expi293F cells with Polyethylenimine (PEI, Polysciences). The supernatants of cultured cells were harvested six days post-transfection for purification. Then, mAbs were purified by protein A Resin (smart-lifesciences) and eluted with 0.1 M glycine pH 2.7. The elution containing the mAbs was exchanged into PBS buffer using a 30 kDa ultrafiltration tube (Millipore).

Biolayer interferometry (BLI) assay

The competition between NiV G mAbs was detected by BLI using an Octet-Red96 device (Pall ForteBio). Briefly, 10 μg/mL of the first mAb was loaded onto Octet ProA Biosensors (Sartorius) for 10 min. After a 10 s washing in running buffer (10 mM HEPES pH 7.4, 150 mM NaCl, 3 mM EDTA, 0.05% Tween-20, and 1% BSA), the biosensor tips were dipped into the running buffer containing 500 nM NiV sG for 120 s. Then, the biosensors were dipped into a buffer containing 10 μg/mL of the second mAb or the same first mAb as a control for 120 s. The biosensors were regenerated with 10 mM glycine (pH 2.0). The running buffer was used to define the background.

For antigenic stability detection of the NiV G-ferritin, 10 μg/mL of NiV mAbs HENV-26 or nAH1.3 were loaded on the protein A biosensors for 10 min. Then, the biosensors were dipped into buffer containing the analytes (NiV G-ferritin, NiV G-ferritin-AddaVax, or NiV G-ferritin-alum) which have been stored at 4 °C, 27 °C, 37 °C or 80 °C for different times, and the maximum binding signals (R_{max}) was recorded and normalized by loading signals of HENV-26 or nAH1.3. The relative binding percentage of each sample was calculated by dividing the R_{max} of the tested sample to the R_{max} of corresponding samples stored at −80 °C, and the maximum binding signal of samples stored at −80 °C was defined as 100%.

Competition ELISA of the sera from immunized mice with NiV G mAbs

96-well ELISA plates (Corning) were coated with 3 μg/mL of NiV sG proteins overnight at 4 °C in coating buffer, and then plates were blocked with 50 μL of blocking buffer for 2 h at 37 °C. Sera, collected on Day 61 after the final vaccination, were diluted 100-fold in blocking buffer, added to the wells, and incubated at 37 °C for 1.5 h. Wells with blocking buffer (without serum) served as controls, with their OD450 values defined as 100%. NiV G monoclonal antibodies from different groups were diluted to 0.05 μg/mL and added to the wells for a 25-minute incubation at 37 °C. Plates were washed four times in PBS-T, followed by adding 50 μL HRP goat anti-Human IgG (ABclonal, AS002) for 1 h at 37 °C. Plates were washed, colored, stopped, and read as described above in antigenicity detection ELISA. In another competition ELISA, after blocking, 10 μg/mL of NiV G mAbs from different groups or a negative control mAb T3D9 were added to the plates. Then the sera from NiV sG or NiV G-ferritin vaccinated mice (20000-fold dilution) were added for binding, and the HRP goat anti-mouse IgG (Thermo Scientific, #31430) was used as the detection antibody.

Data availability

All data supporting the conclusions in the paper are present in the paper or the supplementary information.

Received: 14 February 2024; Accepted: 19 August 2024;
Published online: 31 August 2024

References

1. Centers for Disease Control and Prevention (CDC). Outbreak of Hendra-like virus--Malaysia and Singapore, 1998-1999. *MMWR Morb. Mortal. Wkly Rep.* **48**, 265–269 (1999).
2. Centers for Disease Control and Prevention (CDC). Update: outbreak of Nipah virus--Malaysia and Singapore, 1999. *MMWR Morb. Mortal. Wkly Rep.* **48**, 335–337 (1999).
3. Sharma, V., Kaushik, S., Kumar, R., Yadav, J. P. & Kaushik, S. Emerging trends of Nipah virus: A review. *Rev. Med Virol.* **29**, e2010 (2019).
4. Mishra, G., Prajapat, V. & Nayak, D. Advancements in Nipah virus treatment: Analysis of current progress in vaccines, antivirals, and therapeutics. *Immunology* **171**, 155–169 (2024).
5. Conroy, G. Nipah virus outbreak: what scientists know so far. *Nature*. https://www.nature.com/articles/d41586-023-02967-x (2023).
6. Devnath, P. et al. The pathogenesis of Nipah virus: A review. *Micro. Pathog.* **170**, 105693 (2022).
7. Alam, A. M. Nipah virus, an emerging zoonotic disease causing fatal encephalitis. *Clin. Med.* **22**, 348–352 (2022).
8. Chua, K. B. et al. Nipah virus: a recently emergent deadly paramyxovirus. *Science* **288**, 1432–1435 (2000).
9. Marsh, G. A. et al. Cedar virus: a novel Henipavirus isolated from Australian bats. *PLoS Pathog.* **8**, e1002836 (2012).
10. Wu, Z. et al. Novel Henipa-like virus, Mojiang Paramyxovirus, in rats, China, 2012. *Emerg. Infect. Dis.* **20**, 1064–1066 (2014).
11. Zhang, X. A. et al. A Zoonotic Henipavirus in Febrile Patients in China. *N. Engl. J. Med* **387**, 470–472 (2022).
12. Harcourt, B. H. et al. Genetic characterization of Nipah virus, Bangladesh, 2004. *Emerg. Infect. Dis.* **11**, 1594–1597 (2005).
13. Field, H. et al. The natural history of Hendra and Nipah viruses. *Microbes Infect.* **3**, 307–314 (2001).
14. WHO. Nipah virus, https://www.who.int/news-room/fact-sheets/detail/nipah-virus (2018).
15. Bowden, T. A. et al. Structural basis of Nipah and Hendra virus attachment to their cell-surface receptor ephrin-B2. *Nat. Struct. Mol. Biol.* **15**, 567–572 (2008).
16. Xu, K. et al. Host cell recognition by the henipaviruses: crystal structures of the Nipah G attachment glycoprotein and its complex with ephrin-B3. *Proc. Natl Acad. Sci. USA* **105**, 9953–9958 (2008).
17. Liu, Q. et al. Unraveling a three-step spatiotemporal mechanism of triggering of receptor-induced Nipah virus fusion and cell entry. *PLoS Pathog.* **9**, e1003770 (2013).
18. Liu, Q. et al. Nipah virus attachment glycoprotein stalk C-terminal region links receptor binding to fusion triggering. *J. Virol.* **89**, 1838–1850 (2015).
19. Lu, M. et al. Vaccines based on the fusion protein consensus sequence protect Syrian hamsters from Nipah virus infection. *JCI Insight* **8**, e175461 (2023).
20. Bossart, K. N. et al. A Hendra virus G glycoprotein subunit vaccine protects African green monkeys from Nipah virus challenge. *Sci. Transl. Med.* **4**, 146ra107 (2012).
21. Lo, M. K. et al. Evaluation of a Single-Dose Nucleoside-Modified Messenger RNA Vaccine Encoding Hendra Virus-Soluble Glycoprotein Against Lethal Nipah virus Challenge in Syrian Hamsters. *J. Infect. Dis.* **221**, S493–s498 (2020).
22. Walpita, P. et al. A VLP-based vaccine provides complete protection against Nipah virus challenge following multiple-dose or single-dose vaccination schedules in a hamster model. *NPJ Vaccines* **2**, 21 (2017).
23. Mire, C. E. et al. Use of Single-Injection Recombinant Vesicular Stomatitis Virus Vaccine to Protect Nonhuman Primates Against Lethal Nipah Virus Disease. *Emerg. Infect. Dis.* **25**, 1144–1152 (2019).
24. van Doremalen, N. et al. A single-dose ChAdOx1-vectored vaccine provides complete protection against Nipah Bangladesh and Malaysia in Syrian golden hamsters. *PLoS Negl. Trop. Dis.* **13**, e0007462 (2019).
25. Foster, S. L. et al. A recombinant VSV-vectored vaccine rapidly protects nonhuman primates against lethal Nipah virus disease. *Proc. Natl Acad. Sci. USA* **119**, e2200065119 (2022).
26. Lu, M. et al. Both chimpanzee adenovirus-vectored and DNA vaccines induced long-term immunity against Nipah virus infection. *NPJ Vaccines* **8**, 170 (2023).
27. Weingartl, H. M. et al. Recombinant nipah virus vaccines protect pigs against challenge. *J. Virol.* **80**, 7929–7938 (2006).
28. Guillaume, V. et al. Nipah virus: vaccination and passive protection studies in a hamster model. *J. Virol.* **78**, 834–840 (2004).
29. Woolsey, C. et al. Recombinant vesicular stomatitis virus-vectored vaccine induces long-lasting immunity against Nipah virus disease. *J. Clin. Invest.* **133**, e164946 (2023).
30. Cho, K. J. et al. The crystal structure of ferritin from Helicobacter pylori reveals unusual conformational changes for iron uptake. *J. Mol. Biol.* **390**, 83–98 (2009).
31. Gao, X. et al. Nanovaccines for Advancing Long-Lasting Immunity against Infectious Diseases. *ACS Nano* **17**, 24514–24538 (2023).
32. Kelly, H. G., Kent, S. J. & Wheatley, A. K. Immunological basis for enhanced immunity of nanoparticle vaccines. *Expert Rev. Vaccines* **18**, 269–280 (2019).

33. Cohen, A. A. et al. Mosaic nanoparticles elicit cross-reactive immune responses to zoonotic coronaviruses in mice. *Science* **371**, 735–741 (2021).
34. Kanekiyo, M. et al. Mosaic nanoparticle display of diverse influenza virus hemagglutinins elicits broad B cell responses. *Nat. Immunol.* **20**, 362–372 (2019).
35. Kanekiyo, M. et al. Self-assembling influenza nanoparticle vaccines elicit broadly neutralizing H1N1 antibodies. *Nature* **499**, 102–106 (2013).
36. Boyoglu-Barnum, S. et al. Quadrivalent influenza nanoparticle vaccines induce broad protection. *Nature* **592**, 623–628 (2021).
37. Sun, C. et al. A gB nanoparticle vaccine elicits a protective neutralizing antibody response against EBV. *Cell Host Microbe* **31**, 1882–1897.e1810 (2023).
38. Kanekiyo, M. et al. Rational Design of an Epstein-Barr Virus Vaccine Targeting the Receptor-Binding Site. *Cell* **162**, 1090–1100 (2015).
39. Kang, Y. F. et al. Rapid Development of SARS-CoV-2 Spike Protein Receptor-Binding Domain Self-Assembled Nanoparticle Vaccine Candidates. *ACS Nano* **15**, 2738–2752 (2021).
40. Tai, W. et al. Development of a ferritin-based nanoparticle vaccine against the SARS-CoV-2 Omicron variant. *Signal Transduct. Target Ther.* **7**, 173 (2022).
41. Joyce, M. G. et al. A SARS-CoV-2 ferritin nanoparticle vaccine elicits protective immune responses in nonhuman primates. *Sci. Transl. Med.* **14**, eabi5735 (2022).
42. Walls, A. C. et al. Elicitation of broadly protective sarbecovirus immunity by receptor-binding domain nanoparticle vaccines. *Cell* **184**, 5432–5447.e5416 (2021).
43. Dong, J. et al. Potent Henipavirus Neutralization by Antibodies Recognizing Diverse Sites on Hendra and Nipah Virus Receptor Binding Protein. *Cell* **183**, 1536–1550.e1517 (2020).
44. Borisevich, V. et al. Escape From Monoclonal Antibody Neutralization Affects Henipavirus Fitness In Vitro and In Vivo. *J. Infect. Dis.* **213**, 448–455 (2016).
45. De Benedictis, P. et al. Development of broad-spectrum human monoclonal antibodies for rabies post-exposure prophylaxis. *EMBO Mol. Med.* **8**, 407–421 (2016).
46. Nie, J. et al. Quantification of SARS-CoV-2 neutralizing antibody by a pseudotyped virus-based assay. *Nat. Protoc.* **15**, 3699–3715 (2020).
47. Wang, Z. et al. Architecture and antigenicity of the Nipah virus attachment glycoprotein. *Science* **375**, 1373–1378 (2022).
48. Xu, K. et al. Crystal structure of the Hendra virus attachment G glycoprotein bound to a potent cross-reactive neutralizing human monoclonal antibody. *PLoS Pathog.* **9**, e1003684 (2013).
49. Skowron, K. et al. Nipah Virus-Another Threat From the World of Zoonotic Viruses. *Front. Microbiol.* **12**, 811157 (2021).
50. Firdaus, F. Z., Skwarczynski, M. & Toth, I. Developments in Vaccine Adjuvants. *Methods Mol. Biol.* **2412**, 145–178 (2022).
51. Shah, R. R., Hassett, K. J. & Brito, L. A. Overview of Vaccine Adjuvants: Introduction, History, and Current Status. *Methods Mol. Biol.* **1494**, 1–13 (2017).
52. Kim, D. et al. Self-assembling Gn head ferritin nanoparticle vaccine provides full protection from lethal challenge of Dabie bandavirus in aged ferrets. *mBio* **14**, e0186823 (2023).
53. Brouwer, P. J. M. et al. Lassa virus glycoprotein nanoparticles elicit neutralizing antibody responses and protection. *Cell Host Microbe* **30**, 1759–1772.e1712 (2022).
54. Cohen, A. A. et al. Mosaic RBD nanoparticles protect against challenge by diverse sarbecoviruses in animal models. *Science* **377**, eabq0839 (2022).
55. Swanson, K. A. et al. A respiratory syncytial virus (RSV) F protein nanoparticle vaccine focuses antibody responses to a conserved neutralization domain. *Sci. Immunol.* **5**, eaba6466 (2020).
56. Malonis, R. J. et al. A Powassan virus domain III nanoparticle immunogen elicits neutralizing and protective antibodies in mice. *PLoS Pathog.* **18**, e1010573 (2022).
57. Lefrancios, L. & Lyles, D. S. The interactionof antiody with the major surface glycoprotein of vesicular stomatitis virus. I. Analysis of neutralizing epitopes with monoclonal antibodies. *Virology* **121**, 157–167 (1982).
58. von Boehmer, L. et al. Sequencing and cloning of antigen-specific antibodies from mouse memory B cells. *Nat. Protoc.* **11**, 1908–1923 (2016).

Acknowledgements

We are grateful to Dr. Huan Yan (Wuhan University) and the National Virus Resource Center for the reagents. We appreciate the technical support of Dr. Yin Liu (Medical Research Institute, Wuhan University) in single-cell sorting and Zhou Liang (BEST Science & Technology, Beijing, China) in differential fluorescence scanning. The hamster challenge and live virus neutralization work were conducted at National Biosafety Laboratory, Wuhan, Chinese Academy of Sciences. We are particularly grateful to the running team of National Biosafety Laboratory, Wuhan for their work. This work was supported by the National Key Research and Development Program (2022YFC2604100) and the Hubei Province health and family planning scientific research project (WJ2023Q007) to H.Z., and CAS Pioneer Hundred Talents Program to Z.D.

Author contributions

D.Z., R.C., and Y.Y. are co-first authors of this publication. H.Z., and Z.D. designed and supervised the project. D.Z. conducted the biochemical preparations and functional assays with the help of R.C., G.Z., X.L., B.W., Y.F., and S.Y.; R.C. performed the isolation of NiV G mAbs; D.Z., Y.W., R.C., G.Z., and F.Y. performed the animal experiments in SPF; Y.Y., H.L., G.G., Y.P., X.H., and M.C. performed BSL-4 and ABSL-4 experiments; D.Z., R.C., Z.D. and H.Z. analyzed the data and wrote the manuscript with input from all authors.

Competing interests

The authors declare no competing interests.

Additional information

Supplementary information The online version contains supplementary material available at https://doi.org/10.1038/s41541-024-00954-5.

Correspondence and requests for materials should be addressed to Zengqin Deng or Haiyan Zhao.